A

B

recovery interval at –80 mV and then a second test pulse to +50 mV (P2). Both the inactivation time constants and the time constant for recovery from inactivation were determined by fitting the data to a single exponential (Eq. 3):

$$I(t) \text{ (or P2/P1)} = A + B_{exp}(-t/\tau), \qquad (3)$$

where $I(t)$ = current amplitude at time t, A and B = constants, and τ = inactivation time constant or time constant for recovery from inactivation. For measurement of recovery from inactivation, the plot of P2/P1 instead of $I(t)$ was used.

All data were given as mean ± SEM. Statistical comparisons between two groups were analyzed using Student's unpaired t-test. Comparisons among multiple groups were analyzed using analysis of variance followed by Dunnett test. $P < .05$ was considered significant.

Results

Effects of *KCNE2* on Kv4.3 currents and its gating kinetics

WT *KCNE2* initially was co-expressed with *KCND3*, the gene encoding Kv4.3, the α subunit of the I_{to} channel,[17,18] in CHO cells. Figure 1A shows representative whole-cell current traces recorded from cells transfected with *KCND3* and co-transfected with (right) or without (left) *KCNE2*.

Cells expressing Kv4.3 channels alone showed rapidly activating and inactivating currents. Co-expression of *KCNE2* significantly reduced peak current densities as summarized in the current–voltage relationship curve shown in Figure 1B and slowed both activation and inactivation kinetics (Table 1). Figure 1C (left) shows mean time intervals from the onset of the pulse to maximum current (time to peak), whereas the right panel shows time constants of inactivation (at +20 mV) obtained using Equation 3. Thus, co-transfection of *KCNE2* significantly increased both the time to peak and the time constant.

In contrast, *KCNE2* did not affect the voltage dependence of steady-state activation as assessed by plotting the normalized conductance as a function of test potential (Figure 1D). Fitting to the Boltzmann equation (Eq. 2) yielded half-maximal activation potentials of –6.5 ± 2.1 mV for Kv4.3 alone (open circles) and –5.5 ± 1.7 mV for Kv4.3 + *KCNE2* channels (filled circles, P = NS; Table 1). These findings are consistent with those previously reported for studies using *Xenopus* oocytes, CHO cells, and HEK293 cells.[20,21]
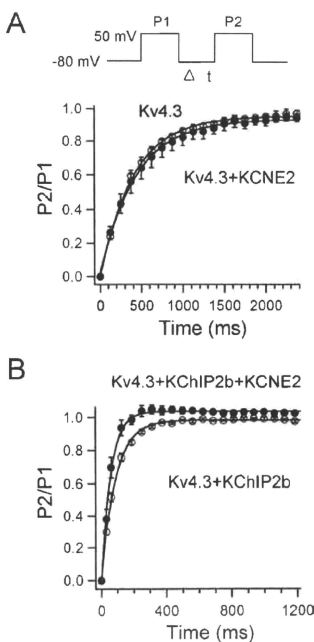
A

B

Figure 3   Effects of *KCNE2* co-expression on recovery from inactivation of Kv4.3 (**A**) and Kv4.3 + KChIP2b (**B**) currents. Recovery from inactivation was assessed by a two-pulse protocol (**A, inset**): a 400-ms test pulse to +50 mV (P1) followed by a variable interval at –80 mV, then by a second test pulse to +50 mV (P2). Data were fit to a single exponential.
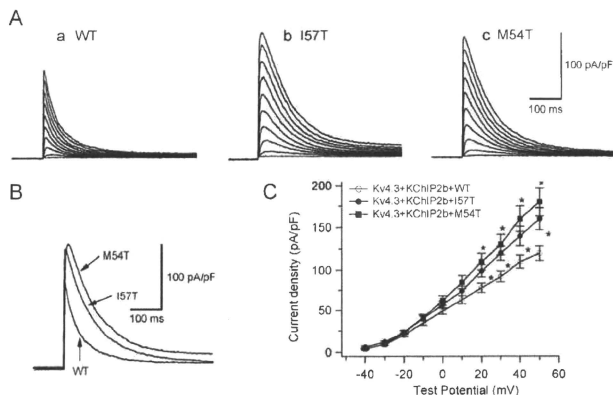
Figure 4   Two *KCNE2* transmembrane variants, I57T and M54T, increase the reconstituted Kv4.3 + KChIP2b channel current and slow its inactivation. **A:** Three sets of current traces elicited by depolarizing pulses for 500 ms from a holding potential of −80 mV to potentials ranging between −40 and +50 mV in 10-mV increments (same protocol as in experiments of Figure 1A). **B:** Superimposition of three original current traces recorded upon depolarization showing variant-related increase in peak outward current density. **C:** Current–voltage relationship curve showing average peak outward current densities (*P <.05 vs Kv4.3 + KChIP2b + WT). WT = wild type.

KCNE2 co-expression also caused a positive shift (approximately +5 mV) of voltage dependence of steady-state inactivation. Steady-state inactivation was assessed using a double-step pulse method (Figure 2A, inset). Peak outward currents recorded at various levels of prepulse (Figure 2A) were normalized by that measured after a 500-ms prepulse at −90 mV and are plotted as a function of prepulse test potentials (Figure 2B). Half-inactivation potentials of steady-state inactivation, determined by fitting data to the Boltzmann equation (Eq. 2), were −46.0 ± 1.3 mV for Kv4.3 (open circles) and −40.8 ± 1.7 mV for Kv4.3 + *KCNE2* (filled circles, P <.01), consistent with the observation of Tseng's group.[13]

A double-pulse protocol (Figure 3A, inset) was used to test the effect of *KCNE2* co-expression on the time course for recovery from inactivation. Figure 3A shows the time course of recovery of Kv4.3 alone (open circles) and Kv4.3 + *KCNE2* (filled circles). Mean time constants for recovery from inactivation were not significantly different, indicating that co-transfection of *KCNE2* did not affect the time course of recovery from inactivation.

Effects of *KCNE2* on Kv4.3 + KChIP2b current and its gating kinetics

For human native cardiac I_{to}, KChIP2 has been shown to serve as a principal β subunit.[22–25] Accordingly, in another series of experiments, we examined the effect of WT and mutant *KCNE2* on Kv4.3 + KChIP2b current. Consistent with previous reports, in the presence of KChIP2, Kv4.3 currents showed a significantly faster recovery from inactivation (Figure 3B and Table 1).[26,27] Co-expression of WT

KCNE2 produced similar changes on Kv4.3 + KChIP2b current as on Kv4.3 current (Table 1). Kv4.3 + KChIP2b current recovery from inactivation was further accelerated: average time constant was 89.2 ± 6.5 ms for Kv4.3 + KChIP2b alone (open circles) and 60.2 ± 8.4 ms for Kv4.3 + KChIP2b + *KCNE2* (filled circles, P <.05). In 16 of 21 cells transfected with *KCNE2*, we observed an "overshoot" phenomenon, which is commonly seen during recording of native I_{to} in human ventricular myocytes.[28]

KCNE2 variants increase Kv4.3 + KChIP2b current and alter its gating kinetics

The I57T variant was first identified in an asymptomatic middle-aged woman with very mild QT prolongation.[6] In addition to this variant, the authors reported another *KCNE2* variant of the transmembrane segment (M54T) that was associated with ventricular fibrillation during exercise in a middle-aged woman. This patient appeared to show a wide range of QTc interval (390–500 ms). Therefore, we tested the functional effects of these two transmembrane *KCNE2* variants on Kv4.3 + KChIP2b currents.

The three panels of Figure 4A show three sets of current traces elicited by depolarizing pulses from a holding potential of −80 mV in cells co-transfected with WT (a), I57T (b), or M54T (c) *KCNE2*. Neither variant caused a significant shift of half-maximal activation voltage: −7.4 ± 1.4 mV (n = 8) for co-expression of WT *KCNE2*, −6.1 ± 1.5 mV (n = 8) for I57T, and −6.6 ± 1.6 mV (n = 8) for M54T. Both variants significantly increased I_{to} density: 125.0 ± 10.6 pA/pF in WT *KCNE2* (n = 21), 178.1 ± 12.1 pA/pF with I57T (n = 9), and 184.3 ± 27.9 pA/pF with M54T (n = 9, Figure 4C).
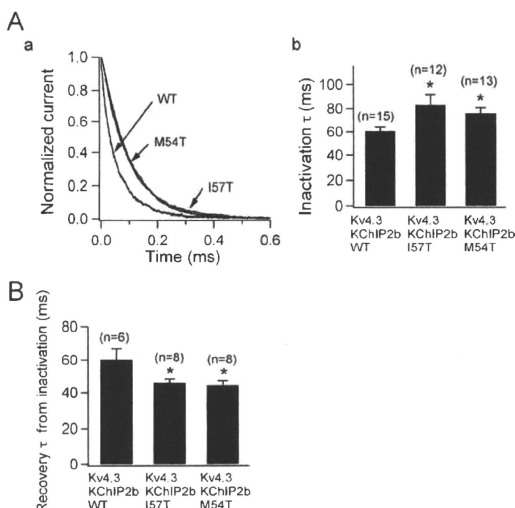
Figure 5   Two *KCNE2* variants slow inactivation kinetics and accelerate recovery from inactivation. **A, a:** Three current traces obtained from Chinese hamster ovary (CHO) cells transfected with wild-type (WT), I57T, and M54T *KCNE2* variant co-expressed with Kv4.3 and KChIP2b. Traces, which are normalized and superimposed, show that the variants slow inactivation. **A, b:** Time constants of decay at $+20$ mV for WT and variant *KCNE2* (*$P <.05$ vs Kv4.3 + KChIP2b + WT). Numbers in parentheses indicate numbers of observations. **B:** Time constants of recovery from inactivation recorded using a double-pulse protocol (*$P <.05$ vs Kv4.3 + KChIP2b + WT). Numbers in parentheses indicate numbers of observations.

Figure 5A shows the three traces depicted in Figure 4B normalized to their peak current level. This representation shows that the time course of inactivation of the two variant currents is slowed. The current decay was fitted by Equation 3 and the time constants (at $+20$ mV) summarized in Figure 5A, panel b. Finally, Figure 5B shows that the time constants of recovery of the two mutant channels from inactivation were significantly reduced. Thus, compared to WT *KCNE2*, recovery of reconstituted Kv4.3 + KChIP2b channels from inactivation was significantly accelerated with both I57T and M54T mutants.

Discussion

Kv4.3/KChIP2/MiRP1 complex can recapitulate the native I_{to}

In the present study, co-expression of WT *KCNE2* produced changes in kinetic properties (Figures 1–3) that led to close recapitulation of native cardiac I_{to}.[28,29] Notably, in addition to causing a positive shift of steady-state inactivation (Figure 2), *KCNE2* co-expression hastened the recovery of Kv4.3 + KChIP2b channels from inactivation (Figure 3). These modifications rendered Kv4.3 + KChIP2b channels more similar to native cardiac I_{to}, suggesting that *KCNE2* may be an important component of the native I_{to} channel complex. In contrast to a previous observation in HEK293 cells,[21] *KCNE2* co-expression decreased the current

density of Kv4.3 and Kv4.3 + KChIP2b channel current in the present study, which seems to be a more reasonable result as the native I_{to} density reportedly was smaller in isolated human heart.[28] *KCNE2* co-expression has also been shown to reduce the density of Kv7.1[8,9] and HERG[6,7] channels.

Similar to the result of Deschenes and Tomaselli,[21] we failed to observe an overshoot during recovery from inactivation when *KCNE2* was co-expressed with Kv4.3 (Figure 3A), which is in contrast to the report of another group.[13] However, co-expression of *KCNE2* with Kv4.3 + KChIP2 channels produced an overshoot (Figure 3B), consistent with the report of Wettwer's group.[25] Wettwer et al also found that other *KCNE* subunits either were ineffective or induced only a small overshoot in CHO cells. Therefore, both MiRP1 and KChIP2 subunits are sufficient and necessary to recapitulate native I_{to} in the heart. Considering that the overshoot phenomenon has been described only in human ventricular I_{to} channels of the epicardial but not endocardial region,[28] these results may further implicate participation of MiRP1 and KChIP2 in the I_{to} channel complex in epicardium.

KCNE2 variants may alter the arrhythmogenic substrate by modulating I_{to}

Heterologous expression in CHO cells was conducted to examine the functional effects of I57T and M54T variants on Kv4.3 + KChIP2 channels. Both I57T and M54T

KCNE2 variants significantly (1) increased peak transient outward current density (Figure 4), (2) slowed the decay of the reconstituted I_{to} (Figure 5A), and (3) accelerated its recovery from inactivation (Figure 5B). Both variants thus caused an important gain of function in human I_{to}. These sequence changes may play a role in modulating I_{to} and thereby predispose to some inherited fatal rhythm disorders.

Functional effects on I_{to} induced by I57T and M54T resemble each other, increasing I_{to} density and accelerating its recovery from inactivation. The gain of function in I_{to} opposes the fast inward Na^+ currents during phase 0 of the action potential, leading to all or none repolarization at the end of phase 1 and loss of the epicardial action potential dome, thus promoting phase 2 reentry and fatal ventricular arrhythmias.[30]

Another *KCNE2* variant (M54T) associated with fatal arrhythmias was first identified in a woman who had a history of ventricular fibrillation and varied QT intervals.[6] It is possible that her arrhythmia was also related to a gain of function in I_{to} secondary to this variation in *KCNE2*. Interestingly, the I57T variant has been reported to produce a loss of function of HERG or Kv7.1 channels, thereby predisposing to long QT syndrome,[6,8] indicating that the same *KCNE2* variant could cause two different cardiac rhythm disorders, similar to long QT syndrome and Brugada syndrome caused by *SCN5A* mutations.[31,32]

References

1. Kass RS, Freeman LC. Potassium channels in the heart: cellular, molecular, and clinical implications. Trends Cardiovasc Med 1993;3:149–159.

2. MacKinnon R. Determination of the subunit stoichiometry of a voltage-activated potassium channel. Nature 1991;350:232–235.

3. Abbott GW, Goldstein SA. A superfamily of small potassium channel subunits: form and function of the MinK-related peptides (MiRPs). Q Rev Biophys 1998;31:357–398.

4. Barhanin J, Lesage F, Guillemare E, Fink M, Lazdunski M, Romey G. KvLQT1 and IsK (minK) proteins associate to form the I_{Ks} cardiac potassium current. Nature 1996;384:78–80.

5. Sanguinetti MC, Curran ME, Zou AR, et al. Coassembly of KvLQT1 and minK (I_{Ks}) proteins to form cardiac I_{Ks} potassium channel. Nature 1996; 384:80–83.

6. Abbott GW, Sesti F, Splawski I, et al. MiRP1 forms I_{Kr} potassium channels with HERG and is associated with cardiac arrhythmia. Cell 1999;97:175–187.

7. Sesti F, Abbott GW, Wei J, et al. A common polymorphism associated with antibiotic-induced cardiac arrhythmia. Proc Natl Acad Sci U S A 2000;97: 10613–10618.

8. Tinel N, Diochot S, Borsotto M, Lazdunski M, Barhanin J. *KCNE2* confers background current characteristics to the cardiac KCNQ1 potassium channel. EMBO J 2000;19:6326–6330.

9. Wu DM, Jiang M, Zhang M, Liu XS, Korolkova YV, Tseng GN. *KCNE2* is colocalized with KCNQ1 and *KCNE1* in cardiac myocytes and may function as a negative modulator of $I(K_s)$ current amplitude in the heart. Heart Rhythm 2006;3:1469–1480.

10. Toyoda F, Ueyama H, Ding WG, Matsuura H. Modulation of functional properties of KCNQ1 channel by association of KCNE1 and KCNE2. Biochem Biophys Res Commun 2006;344:814–820.

11. Yu H, Wu J, Potapova I, et al. MinK-related peptide 1: a beta subunit for HCN ion channel subunit family enhances expression and speeds activation. Circ Res 2001;88:E84–E87.

12. McCrossan ZA, Roepke TK, Lewis A, Panaghie G, Abbott GW. Regulation of the Kv2.1 potassium channel by MinK and MiRP1. J Membr Biol 2009;228:1–14.

13. Zhang M, Jiang M, Tseng GN. MinK-related peptide 1 associates with Kv4.2 and modulates its gating function: potential role as beta subunit of cardiac transient outward channel? Circ Res 2001;88:1012–1019.

14. Delpon E, Cordeiro JM, Nunez L, et al. Functional effects of KCNE3 mutation and its role in the development of Brugada syndrome. Circ Arrhythm Electrophysiol 2008;1:209–218.

15. Roepke TK, Kontogeorgis A, Ovanez C, et al. Targeted deletion of *KCNE2* impairs ventricular repolarization via disruption of $I_{K,slow1}$ and $I_{to,f}$. FASEB J 2008;22:3648–3660.

16. Calloe K, Cordeiro JM, Di Diego JM, et al. A transient outward potassium current activator recapitulates the electrocardiographic manifestations of Brugada syndrome. Cardiovasc Res 2009;81:686–694.

17. Dixon JE, Shi W, Wang HS, et al. Role of the Kv4.3 K^+ channel in ventricular muscle. A molecular correlate for the transient outward current. Circ Res 1996;79:659–668.

18. Kääb S, Dixon J, Duc J, et al. Molecular basis of transient outward potassium current downregulation in human heart failure: a decrease in Kv4.3 mRNA correlates with a reduction in current density. Circulation 1998;98:1383–1393.

19. Benitah JP, Gomez AM, Bailly P, et al. Heterogeneity of the early outward current in ventricular cells isolated from normal and hypertrophied rat hearts. J Physiol 1993:469:111–138.

20. Singleton CB, Valenzuela SM, Walker BD, et al. Blockade by N-3 polyunsaturated fatty acid of the Kv4.3 current stably expressed in Chinese hamster ovary cells. Br J Pharmacol 1999;127:941–948.

21. Deschênes I, Tomaselli GF. Modulation of Kv4.3 current by accessory subunits. FEBS Lett 2002;528:183–188.

22. Wang S, Bondarenko VE, Qu Y, Morales MJ, Rasmusson RL, Strauss HC. Activation properties of Kv4.3 channels: time, voltage and $[K^+]_o$ dependence. J Physiol 2004;557:705–717.

23. An WF, Bowlby MR, Betty M, et al. Modulation of A-type potassium channels by a family of calcium sensors. Nature 2000;403:553–556.

24. Decher N, Uyguner O, Scherer CR, et al. hKChIP2b is a functional modifier of hKv4.3 potassium channels: cloning and expression of a short hKChIP2b splice variant. Cardiovasc Res 2001;52:255–264.

25. Radicke S, Cotella D, Graf EM, et al. Functional modulation of the transient outward current I_{to} by *KCNE* beta-subunits and regional distribution in human non-failing and failing hearts. Cardiovasc Res 2006;71:695–703.

26. Deschênes I, DiSilvestre D, Juang GJ, Wu RC, An WF, Tomaselli GF. Regulation of Kv4.3 current by KChIP2b splice variants: a component of native cardiac I_{to}? Circulation 2002;106:423–429.

27. Radicke R, Vaquero M, Caballero R, et al. Effects of MiRP1 and DPP6 β-subunits on the blockade induced by flecainide of Kv4.3/KChIP2 channels. Br J Pharmacol 2008;154:774–786.

28. Wettwer E, Amos GJ, Posival H, Ravens U. Transient outward current in human ventricular myocytes of subepicardial and subendocardial origin. Circ Res 1994; 75:473–482.

29. Patel SP, Campbell DL. Transient outward potassium current, "I_{to}," phenotypes in the mammalian left ventricle: underlying molecular, cellular and biophysical mechanisms. J Physiol 2005;569:7–39.

30. Antzelevitch C. Brugada syndrome. Pacing Clin Electrophysiol 2006;29:1130–1159.

31. Bezzina C, Veldkamp MW, van den Berg MP, et al. A single Na^+ channel mutation causing both long-QT and Brugada syndromes. Circ Res 1999;85:1206–1213.

32. Van den Berg MP, Wilde AA, Viersma TJW, et al. Possible bradycardic mode of death and successful pacemaker treatment in a large family with features of long QT syndrome type 3 and Brugada syndrome. J Cardiovasc Electrophysiol 2001;12:630–636.

Neurally Mediated Syncope as a Cause of Syncope in Patients With Brugada Electrocardiogram

MIKI YOKOKAWA, M.D., HIDEO OKAMURA, M.D., TAKASHI NODA, M.D., PH.D.,
KAZUHIRO SATOMI, M.D., PH.D., KAZUHIRO SUYAMA, M.D., PH.D.,
TAKASHI KURITA, M.D., PH.D., NAOHIKO AIHARA, M.D., SHIRO KAMAKURA, M.D., PH.D.,
and WATARU SHIMIZU, M.D., PH.D.

From the Division of Cardiology, Department of Internal Medicine, National Cardiovascular Center, Suita, Japan

Neurally Mediated Syncope in Brugada Syndrome. *Introduction:* Patients with type 1 Brugada electrocardiogram (ECG) and an episode of syncope are diagnosed as symptomatic Brugada syndrome; however, all episodes of syncope may not be due to ventricular tachyarrhythmia.

Methods and Results: Forty-six patients with type 1 Brugada ECG (all males, 51 ± 13 years, 29 spontaneous, 17 Ic-drug induced), 20 healthy control subjects (all males, 35 ± 11 years), and 15 patients with suspected neurally mediated syncope (NMS; 9 males, 54 ± 22 years) underwent the head-up tilt (HUT) test. During the HUT test, 12-lead ECGs were recorded in all patients, and the heart rate variability was investigated in some patients. Sixteen (35%) of 46 patients with Brugada ECG, 2 (10%) of 20 control subjects, and 10 (67%) of 15 patients with suspected NMS showed positive responses to the HUT test. Although no significant differences were observed in HUT-positive rate among Brugada patients with documented VT (7/14; 50%), syncope (5/19; 26%) and asymptomatic patients (4/13; 31%), the HUT-positive rate was significantly higher in patients with documented VT (50%) and those with VT or no symptoms (11/27, 41%) compared to that in control subjects (10%) (P < 0.05). Augmentation of ST-segment amplitude (≥ 0.05 mV) in leads V1-V3 was observed in 11 (69%) of 16 HUT-positive patients with Brugada ECG during vasovagal responses, and was associated with augmentation of parasympathetic tone following sympathetic withdrawal.

Conclusion: Thirty-five percent of patients with Brugada ECG showed vasovagal responses during the HUT test, suggesting that some Brugada patients have impaired balance of autonomic nervous system, which may relate to their syncopal episodes. *(J Cardiovasc Electrophysiol, Vol. 21, pp. 186-192, February 2010)*

autonomic nervous system, Brugada syndrome, head-up tilt test, syncope, sudden death

Introduction

Brugada syndrome is characterized by ST-segment elevation in the right precordial leads V1 through V3 and an episode of ventricular tachyarrhythmia (VT) in the absence of structural heart disease.[1-3] In patients with Brugada syndrome, syncopal episodes are generally thought to be due to VT; however, all episodes of syncope may not be owing to VT events. Neurally mediated syncope (NMS) is 1 of the causes of syncope in general population, and it refers to a reflex response that some triggering factors give rise to arterial vasodilatation associated with relative or absolute bradycar-

dia.[4] In general, the overall prognosis in patients with NMS is quite favorable.[4] On the other hand, the precise cause of syncope in patients with Brugada syndrome is difficult to determine. Therefore, the therapeutic strategy for Brugada patients with syncope is often problematic. The aim of this study was to evaluate the possibility of NMS as a cause of syncope in patients with Brugada electrocardiogram (ECG).

Methods

Patients Population

The study population consisted of 46 consecutive patients with type 1 Brugada ECG who were admitted to the National Cardiovascular Center, Suita, Japan, between May 2004 and March 2006 (all males, ages 26 to 77; mean 51 ± 13 years, 29 spontaneous, 17 Ic-drug induced), 20 healthy control subjects (all males, 35 ± 11 years), and 15 patients suspected of NMS (9 males, 54 ± 22 years). Ethical approval was obtained from the Institutional Review Committee of our hospital, and all patients and control subjects gave their informed, written consent before participation. The control subjects and the patients with suspected NMS showed no structural heart diseases, normal physical examination results, and normal 12-lead ECGs, and received no drug treatment affecting the sympathetic nervous system. Type 1 Brugada ECG was defined as a coved type ST-segment elevation of ≥ 0.2 mV at

J point observed in more than 1 of the right precordial leads (V1 to V3) in the presence or absence of a sodium channel blocker.[2]

Head-Up Tilt Test

The HUT test was performed in the afternoon after 4 hours of fasting in a quiet and comfortable room equipped for cardiopulmonary resuscitation. All patients were allowed to lie on an electrically controlled tilt table an intravenous line containing 5% dextrose was inserted into 1 arm, and allowed to rest in supine position for at least 10 minutes. A positive HUT test was defined by the development of syncope or presyncope associated with relative bradycardia ($\geq$20% decrease in heart rate compared with baseline) or hypotension (systolic blood pressure <80 mmHg). Presyncope was defined as the induction of symptoms of imminent syncope, and syncope was defined as sudden transient loss of consciousness. Positive response to the HUT test was classified into 3 types owing to hemodynamic status, such as vasodepressor type (hypotension without significant bradycardia), cardioinhibitory type (bradycardia without associated hypotention), and mixed type (hypotension followed by bradycardia).[4] At first, we performed passive tilt (Control-Tilt) at an angle of 70 degrees for 30 minutes. When Control-Tilt was negative, sublingual nitroglycerin (NTG) spray 0.3 mg was administered, and the test was continued for 15 minutes (NTG-Tilt). The endpoint of each tilt test was the time when patients showed positive responses or the completion of HUT-protocol.

Parameters Measured During the Head-Up Tilt Test

Heart rate and blood pressure

Heart rate was monitored, and cuff blood pressure was measured by electrosphygmomanometry with a microphone placed over the brachial artery to detect Korotkoff sounds every minute (STBP-780, Colin Electronics, Komaki, Japan) in all patients during the HUT test.

ST-segment amplitude in the right precordial leads

Twelve-lead ECGs were recorded every 1 minute during the HUT test, and the changes of ST-segment amplitude in the right precordial leads (V1-V3) were analyzed (ML-6500, Fukuda-denshi, Tokyo, Japan) in all patients during the HUT test.

Heart rate variability

Six-lead ECGs from the Task Force Monitor (CNSystem, Graz, Austria)[5-7] were measured for beat-to-beat heart rate and consecutive R-R intervals in 10 patients with Brugada ECG (4 documented VT, 5 syncopal episode only, and 1 asymptomatic), 9 control subjects, and 5 patients with suspected NMS. The heart rate variability (HRV) was investigated by a power spectral analysis delineating the low-frequency component (LF; 0.04–0.15 Hz) and the high-frequency component (HF; 0.15–0.40 Hz).[8] We analyzed the normalized unit of the HF components (%) calculated automatically (HF/power spectral density-very low-frequency component [0–0.04 Hz] × 100)[8,9] and the LF/HF ratio. The HF indicates the tone of the parasympathetic nervous system, and the LF/HF ratio indicates the sympathovagal balance.

Statistical Analysis

Numerical values were expressed as means ± SD unless otherwise indicated. Comparisons of parameters between 2 groups were made using the unpaired Student *t*-test. Comparisons of parameters among 3 groups were made with a one-way analysis of variance (ANOVA), followed by the Scheffe's multiple-comparison test. Categorical variables were compared using a chi-square analysis using the Yate's correction or Fisher exact test if necessary. An overall chi-square test for a 2 × n table was performed when comparisons involved >2 groups. A P-value < 0.05 was considered significant.

Results

Clinical Characteristics

The clinical characteristics of 46 patients with Brugada ECG and 15 patients with suspected NMS are shown in Table 1. The patients with Brugada ECG were divided into 3 groups: (1) 14 patients with documented VT; (2) 19 patients with syncopal episodes only; and (3) 13 asymptomatic patients. No significant differences were observed in age, incidence of spontaneous type 1 ECG, family history of sudden cardiac death (SCD), induced ventricular fibrillation during electrophysiologic study (EPS), and *SCN5A* mutation. Implantable cardioverter-defibrillator (ICD) was implanted more frequently in patients with documented VT. The triggers of VT and/or syncope are also shown in Table 1. Seventy-nine percent of VT episodes occurred during sleep or at rest in patients with documented VT (P < 0.0001 vs the patients with syncopal episodes only and suspected NMS). On the other hand, in patients with syncopal episodes only, 15% of syncopal episodes occurred after urination, 21% during standing, and 21% after drinking alcohol, which seemed to be similar patterns in patients with suspected NMS. Based on the clinical description of the syncopal events, 16 (84%) of 19 Brugada patients with syncopal episodes were suspected to have NMS. Syncopal episodes seemed to be due to VT in 1 of the remaining 3 patients.

Positive Response to the Head-Up Tilt Test

Comparison of the positive responses to the HUT test between 46 patients with Brugada ECG and 20 control subjects along with 15 patients with suspected NMS are shown in Table 2. Sixteen (35%) of 46 patients with Brugada ECG showed positive responses. Positive responses were developed in 1 (2%) of 46 patients during Control-Tilt and in 15 (33%) of 45 patients during NTG-Tilt, and the mixed type was predominant (94%). In patients with Brugada ECG, there were no significant differences in the incidence of positive responses among patients with documented VT (50%), those with syncopal episodes only (26%), and asymptomatic patients (31%). No significant differences were observed in the type of positive responses between the 3 groups. The mixed type was predominant (100%, 100%, and 75%, respectively), and cardioinhibitory type was not observed in all 3 groups. Two (10%) of 20 control subjects and 10 (67%) of 15 patients with suspected NMS showed positive responses. The HUT-positive rate was not significantly different between all 46 patients with Brugada ECG, 20 control subjects and 15 subjects with suspected NMS (35% vs 10% vs 67%);

TABLE 1

Clinical Characteristics of Patients with Brugada Electrocardiogram and Suspected NMS

	Documented VT (n = 14)	Syncopal Episodes only (n = 19)	Asymptomatic (n = 13)	Suspected NMS (n = 15)
Age (years)	50 ± 15	51 ± 12	52 ± 14	54 ± 22
Spontaneous type 1 ECG	10 (71)	9 (47)	10 (77)	–
Family history of SCD	4 (29)	4 (21)	4 (31)	–
Induced VF during EPS	10/12 (83)	15/18 (83)	8/11 (73)	–
SCN5A mutation	1 (7)	3 (16)	0 (0)	–
ICD implantation	14 (100)	13 (68)*	7 (54)*	–
Triggers of syncope				
During sleeping or at rest	11 (79)	1 (5)*	–	0*
After urination	0	3 (15)	–	1 (7)
Prolonged standing at attention	0	4 (21)	–	4 (27)
After drinking alcohol	0	4 (21)	–	6 (40)
After meal	1 (7)	0	–	0
After exertion	0	2 (11)	–	2 (13)
After sudden unexpected pain	0	2 (11)	–	0
During driving	0	1 (5)	–	0
Others	2 (14)	2 (11)	–	2 (13)

Values are mean ± SD for age, and expressed as frequency (%). *P < 0.05 vs documented VT group. ECG = electrocardiogram; EPS = electrophysiological study; ICD = implantable cardioverter-defibrillator; NMS = neurally mediated syncope; SCD = sudden cardiac death; VT = ventricular tachyarrhythmias; VF = ventricular fibrillation.

however, the HUT-positive rate was significantly higher in 14 patients with documented VT (50%) and 27 patients with VT or no symptoms (41%) compared to that in control subjects (10%) (P = 0.03, P = 0.04, respectively). The HUT-positive rate in 19 Brugada patients with syncopal episodes (26%) was significantly lower than that in 15 patients with suspected NMS (P = 0.04), although the syncopal episodes in 84% of the 19 patients were suspected to be due to NMS. Positive responses to the HUT test were more frequency observed in 15 patients with suspected NMS compared to those in 20 control subjects (10/15 vs 2/20; P < 0.001).

Comparison of the clinical characteristics between 16 HUT-positive patients and 30 HUT-negative patients with Brugada ECG were shown in Table 3. No significant differences were observed in cardiac events, such as documented VT or syncope. Furthermore, there were no significant differences in the clinical characteristics, such as age, spontaneous type 1 ECG, a family history of SCD, inducibility of ventricular fibrillation during EPS, *SCN5A* mutation, and ICD implantation.

Response of Heart Rate and ST-Segment Amplitude

In patients with Brugada ECG, the heart rate was increased by 12 ± 9 beats/min during Control-Tilt, and by 24 ± 14 beats/min during NTG-Tilt. As the heart rate was increased, decrease of ST-segment amplitude of ≥ 0.05 mV from baseline in the right precordial leads was observed in 11 (24%) of 46 patients during Control-Tilt (−0.14 ± 0.08 mV), and in 19 of 45 (42%) patients during NTG-Tilt (−0.15 ± 0.10 mV) (Fig. 1C). However, augmentation of ST-segment amplitude of ≥ 0.05 mV in the right precordial leads was observed just before and after positive responses to the HUT test in 11 (69%) of 16 HUT-positive patients (0.10 ± 0.06 mV) (Figs. 1D and E). These significant ST-segment augmentation was observed in 1 patient during Control-Tilt (documented VT), and 10 patients during NTG-Tilt (5 documented VT, 2 syncopal episodes only, 3 asymptomatic), respectively. On the other hand, augmentation of the ST-segment amplitude of ≥ 0.05 mV was 2 (7%) of 30 HUT-negative patients during NTG-Tilt (1 documented VT, 1 syncopal episodes only). As a result, the average ST-segment augmentation was

TABLE 2

Responses to Head-Up Tilt Test in Patients with Brugada Electrocardiogram, Control Subjects, and Patients with Suspected NMS

	All (n = 46)	Documented VT (n = 14)	Syncopal Episodes Only (n = 19)	Asymptomatic (n = 13)	Brugada ECG with VT or No Symptoms (n = 27)	Control Subjects (n = 20)	Suspected NMS (n = 15)
Age (years)	51 ± 13*	50 ± 15*	51 ± 12*	52 ± 14*	51 ± 14*	35 ± 11	54 ± 22*
Positive response	16 (35)	7 (50)*	5 (26)†	4 (31)	11 (41)*	2 (10)	10 (67)*
Control-tilt	1/45 (2)	1/14 (7)	0/19 (0)	0/13 (0)	1/27 (4)	0/20 (0)	0/15 (0)
NTG-tilt	15/45 (33)†	6/13 (46)*	5/19 (26)†	4/13 (31)	10/26 (38)	2/20 (10)	10/15 (67)*
Type of positive response							
Vasodepressive	1/16 (6)	0	0	1/4 (25)	1/11 (9)	0	1/10 (10)
Cardioinhibitory	0	0	0	0	0	0	0
Mixed	15/16 (94)	7/7 (100)	5/5 (100)	3/4 (75)	10/11 (91)	3 (100)	9/10 (90)

Values are expressed as frequency (%). *P < 0.05 vs control subjects, †P < 0.05 vs suspected NMS. ECG = electrocardiogram; NMS = neurally mediated syncope; NTG = nitroglycerin; VT = ventricular tachyarrhythmias.

TABLE 3

Comparison of Clinical Characteristics Between Head-up Tilt-Positive Patients and Head-up Tilt-Negative Patients

	HUT-Positive (n = 16)	HUT-Negative (n = 30)	P-value
Age (years)	52 ± 13	50 ± 14	0.58
Documented VT	7 (44)	7 (23)	0.15
Syncope only	5 (31)	14 (47)	0.49
Asymptomatic	4 (25)	9 (30)	0.99
Spontaneous type 1 ECG	11 (69)	18 (60)	0.79
Family history of SCD	4 (25)	8 (27)	1.0
Induced VF during EPS	13/15 (87)	20/26 (77)	0.72
SCN5A mutation	1 (6)	3 (10)	1.0
ICD implantation	14 (88)	24 (80)	0.82

Values are expressed as frequency (%). ECG = electrocardiogram; EPS = electrophysiological study; HUT = head-up tilt test; ICD = implantable cardioverter-defibrillator; SCD = sudden cardiac death; VT = ventricular tachyarrhythmias; VF = ventricular fibrillation.

significantly larger in 16 HUT-positive patients than in 30 HUT-negative patients at similar heart rate (0.06 ± 0.06 mV vs −0.04 ± 0.06 mV, P < 0.0001). No ventricular arrhythmias were induced during the HUT test in any patients with Brugada ECG. The ST-segment augmentation was not observed during the HUT test in any control subjects (−0.02 ± 0.02 mV, P < 0.0001 vs 16 HUT-positive Brugada patients) and patients with suspected NMS (−0.02 ± 0.04 mV, P < 0.001 vs 16 HUT-positive Brugada patients; Fig. 2).

Heart Rate Variability and ST-segment Amplitude

Positive responses during NTG-Tilt were observed in 4 (40%) of 10 patients with Brugada ECG, in 1 (11%) of 9 control subjects, and in 4 (80%) of 5 patients with suspected NMS in whom the HRV was monitored. The autonomic ac-

tivities in a representative NTG-Tilt-positive patient with Brugada ECG and those with suspected NMS are shown in Figure 3A and B, respectively. Before positive responses to the HUT test, sympathetic activity (LF/HF ratio) dramatically increased; and then, sympathetic withdrawal occurred immediately. Thereafter, parasympathetic nerve activity (the normalized unit of the HF components) gradually increased. The similar pattern of augmented parasympathetic nerve activity following sympathetic withdrawal during positive responses to the HUT test was observed in all 9 HUT-positive patients. The patterns of HRV were not different among the HUT-positive patients with Brugada ECG, the HUT-positive control subjects, and the HUT-positive patients with suspected NMS. In 3 (75%) of 4 HUT-positive patients with Brugada ECG, the LF/HF ratio decreased and the HF component increased gradually toward the maximum ST-segment elevation just before and after positive response for the HUT test (Fig. 3A), but ST-segment was decreased in patients with NMS (Fig. 3B).
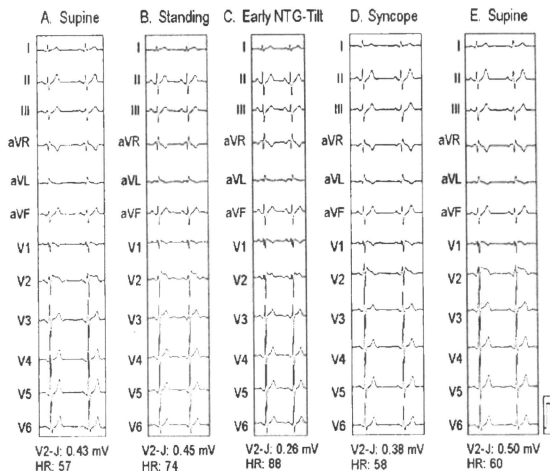
Discussion

In this study, 35% of patients with Brugada ECG showed vasovagal responses during the HUT test regardless of the presence VT or syncope. The HUT test was also positive in 41% among only Brugada patients with documented VT or no symptoms. During vasovagal response, ST-segment augmentation in the right precordial leads (V1-V3) was observed in 11 (69%) of 16 HUT-positive patients with Brugada ECG, but no ventricular arrhythmias were induced in any HUT-positive patients.

Neurally Mediated Syncope as a Cause of Syncope in Brugada Syndrome

Several case reports have described patients exhibiting clinical phenotype of both Brugada syndrome and NMS.[10-12]

Figure 1. *The 12-leads electrocardiogram (ECG) during head-up tilt test in a representative nitroglycerin (NTG)-Tilt-positive patient with type 1 Brugada ECG at supine position (A), at standing position (B), at early phase of NTG-Tilt (C), at syncope (D), and at supine position following syncope (E). The ST-segment elevation was decreased from 0.45 mV to 0.26 mV at early phase of NTG-Tilt as the heart rate was increased (C), while it was augmented to 0.38 mV at syncope (D), and to 0.50 mV at supine position following syncope (E).*
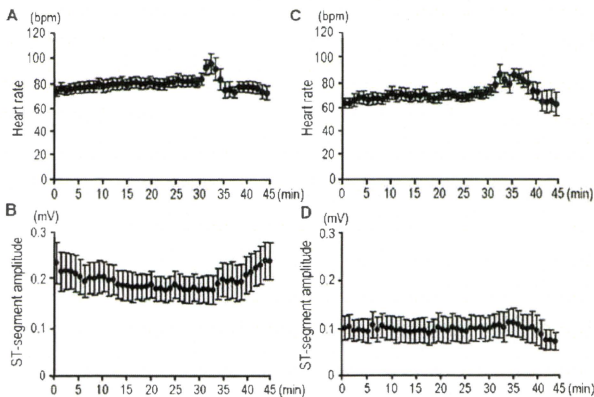
A. Supine   B. Standing   C. Early NTG-Tilt   D. Syncope   E. Supine

V2-J: 0.43 mV   V2-J: 0.45 mV   V2-J: 0.26 mV   V2-J: 0.38 mV   V2-J: 0.50 mV
HR: 57   HR: 74   HR: 88   HR: 58   HR: 60

Figure 2. *Response of the heart rate and ST-segment amplitude during the head-up tilt (HUT) test in 16 HUT-positive patients with Brugada electrocardiogram (ECG) (A, B) and in 10 HUT-positive patients with suspected neurally mediated syncope (NMS) (C, D). At first, the passive tilt (Control-Tilt) was performed for 30 minutes (0–30 minutes). When Control-Tilt was negative, nitroglycerin tilt was continued for 15 minutes (30–45 minutes). The responses of heart rate during positive responses to the HUT test were similar in patients with Brugada ECG (A) to those in patients with suspected NMS (C). In patients with Brugada ECG, ST-segment in lead V2 was augmented before and after positive responses to the HUT test (B), but not in those with suspected NMS (D).*
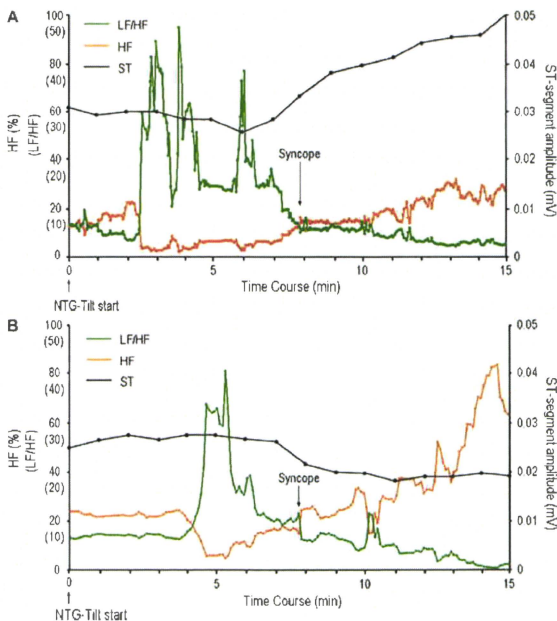

Figure 3. *Autonomic responses during head-up tilt (HUT) test. The autonomic activities in a representative nitroglycerin (NTG)-Tilt-positive patient with type 1 Brugada electrocardiogram (ECG) (A) and those in a representative NTG-Tilt-positive patient with suspected NMS (B). Before tilt-induced syncope, sympathetic activity (LF/HF ratio) dramatically increased; and then, sympathetic withdrawal occurred immediately. Thereafter, parasympathetic nerve activity (the normalized unit of the HF components) gradually increased. In the HUT-positive patient with Brugada ECG, ST-segment augmentation in lead V2 was observed just before and after positive responses, and the LF/HF ratio decreased and the HF component increased gradually toward the maximum ST-segment elevation (A). In contrast, in the HUT-positive patient with suspected NMS, ST-segment amplitude in lead V2 was decreased gradually after positive responses (B).*

It is well known that the autonomic nervous system plays an important role on the arrhythmogenesis of Brugada syndrome. Previous studies showed that the withdrawal of sympathetic activity and the sudden rise in vagal activity was an important triggering factor of ventricular fibrillation.[13-15] Similarly, it has been presumed that parasympathetic tone increase during NMS events in patients with Brugada ECG. Recent basic study showed that *SCN5A*, a major responsible gene in Brugada patients, is expressed not only in the myocardial cells but also in intracardiac ganglia.[16] Makita *et al.* also demonstrated a novel nonsense mutation in *SCN5A* gene in a patient with Brugada syndrome who had been diagnosed as NMS.[17] These results suggested that the abnormal regulation or imbalance of autonomic nervous system may exist regardless of the presence or absence of cardiac events in patients with Brugada ECG.

ST-Segment Elevation in the Precordial Leads During the HUT Test in Patients with Brugada ECG

In Brugada syndrome, spontaneous augmentation of ST-segment elevation occurred along with an increase in vagal activity, especially just before and after the occurrence of ventricular fibrillation.[14] The ST-segment elevation is also known to be modulated by exercise,[18] pharmacological interventions that interact with automatic nervous activities,[19] or taking meals associated with glucose-induced insulin levels.[20] In this study, ST-segment augmentation in the right precordial leads was observed just before and after positive responses to the HUT test in two-thirds (69%) of the HUT-positive patients with Brugada ECG but only in 7% of the HUT-negative patients. In patients with Brugada ECG, the preceding increase of sympathetic nerve activity during the HUT test may cause augmentation of ICa-L, resulting in attenuation of ST-segment elevation.[19] Subsequent augmentation of parasympathetic nerve activity during the HUT test may decrease of ICa-L, and increase Ito, thus augmenting ST-segment amplitude.

Clinical Implication

The second consensus report suggested that symptomatic patients displaying type 1 Brugada ECG (either spontaneous or after class Ic drugs) who present with aborted sudden death should undergo ICD implantation.[3] ICD implantation is also recommended in patients with syncope, seizure, or nocturnal agonal respiration, after noncardiac causes of these symptoms have been carefully ruled out.[3] Needless to say, the ECG recording during syncope is the only convincing way to rule in or out VT during syncope, and only clinical judgment can be used to guide diagnostic and therapeutic decisions. However, in patients with Brugada syndrome, there is an abnormal regulatory imbalance of the autonomic nervous system that may be a common denominator to both syncope and ventricular fibrillation.

Limitations

The control subjects were significantly younger than patients with Brugada ECG or those with suspected NMS. However, it is reported that the positive rate of NTG-Tilt in the elderly was comparable to that seen in younger subjects.[21] Therefore, lower incidence of positive rate of the HUT test in the control subjects than that in the other 2 groups was not due to the relevant difference of age. The incidence of

spontaneous type 1 ECG and the positive rate of the HUT test are smaller in Brugada patients with syncope episodes only than in those with documented VT or asymptomatic patients; however, statistical significance was not observed between the 3 groups.

Conclusions

Thirty-five percent of patients with Brugada ECG showed vasovagal responses during the HUT test. The HUT test was also positive in 41% among only Brugada patients with documented VT or no symptoms. During vasovagal response, ST-segment augmentation in the right precordial leads was observed in 69% of the HUT-positive Brugada patients, but no ventricular arrhythmias were induced. These data suggest that some Brugada patients have impaired balance of autonomic nervous system, which may relate to their syncopal episodes. Additional studies including a large number of subjects are needed to validate our findings and possibly evaluate the role of the HUT test in risk stratification of patients with Brugada ECG.

References

1. Brugada P, Brugada J: Right bundle branch block, persistent ST segment elevation and sudden cardiac death: A distinct clinical and electrocardiographic syndrome. A multicenter report. J Am Coll Cardiol 1992;20:1391-1396.
2. Wilde AA, Antzelevitch C, Borggrefe M, Brugada J, Brugada R, Brugada P, Corrado D, Hauer RN, Kass RS, Nademanee K, Priori SG, Towbin JA, Study Group on the Molecular Basis of Arrhythmias of the European Society of Cardiology: Proposed diagnostic criteria for the Brugada syndrome: Consensus report. Circulation 2002;106:2514-2519.
3. Antzelevitch C, Brugada P, Borggrefe M, Brugada J, Brugada R, Corrado D, Gussak I, LeMarec H, Nademanee K, Perez Riera AR, Shimizu W, Schulze-Bahr E, Tan H, Wilde A: Brugada syndrome: Report of the second consensus conference: Endorsed by the Heart Rhythm Society and the European Heart Rhythm Association. Circulation 2005;111:659-670.
4. Brignole M, Alboni P, Benditt D, Bergfeldt L, Blanc JJ, Bloch Thomsen PE, van Dijk JG, Fitzpatrick A, Hohnloser S, Janousek J, Kapoor W, Kenny RA, Kulakowski P, Moya A, Raviele A, Sutton R, Theodorakis G, Wieling W, Task Force on Syncope, European Society of Cardiology: Guidelines on management (diagnosis and treatment) of syncope. Eur Heart J 2001;22:1256-1306.
5. Nowak L, Nowak FG, Janko S, Dorwarth U, Hoffmann E, Botzenhardt F: Investigation of various types of neurocardiogenic response to head-up tilting by extended hemodynamic and neurohumoral monitoring. Pacing Clin Electrophysiol 2007;30:623-630.
6. Dalla PR, Kleinmann A, Zysk S, Bechtold S, Netz N: Head-up-tilt testing in children: New perspectives using beat-to-beat blood-pressure monitoring. Images Paediatr Cardiol 2005;22:1-7.
7. Boysen A, Lewin MA, Hecker W, Leichter HE, Uhlemann F: Autonomic function testing in children and adolescents with diabetes mellitus. Pediatr Diabetes 2007;8:261-264.
8. Yamasaki F, Sato T, Sugimoto K, Takata J, Chikamori T, Sasaki M, Doi Y: Effect of diltiazem on sympathetic hyperactivity in patients with vasospastic angina as assessed by spectral analysis of arterial pressure and heart rate variability. Am J Cardiol 1998;81:137-140.
9. Pagani M, Lombardi F, Guzzetti S, Rimoldi O, Furlan R, Pizzinelli P, Sandrone G, Malfatto G, Dell'Orto S, Piccaluga E: Power spectral analysis of heart rate and arterial pressure variabilities as a marker of sympatho-vagal interaction in man and conscious dog. Circ Res 1986;59:178-193.
10. Márquez MF, Rivera J, Hermosillo AG, Iturralde P, Colín L, Moragrega JL, Cárdenas M: Arrhythmic storm responsive to quinidine in a patient with Brugada syndrome and vasovagal syncope. Pacing Clin Electrophysiol 2005;28:870-873.
11. Patruno N, Pontillo D, Anastasi R, Sunseri L, Giamundo L, Ruggeri G: Brugada syndrome and neurally mediated susceptibility. Ital Heart J 2005;6:761-764.

12. Samniah N, Iskos D, Sakaguchi S, Lurie KG, Benditt DG: Syncope in pharmacologically unmasked Brugada syndrome: Indication for an implantable defibrillator or an unresolved dilemma? Europace 2001;3:159-163.

13. Wichter T, Matheja P, Eckardt L, Kies P, Schäfers K, Schulze-Bahr E, Haverkamp W, Borggrefe M, Schober O, Breithardt G, Schäfers M: Cardiac autonomic dysfunction in Brugada syndrome. Circulation 2002;105:702-706.

14. Kasanuki H, Ohnishi S, Ohtuka M, Matsuda N, Nirei T, Isogai R, Shoda M, Toyoshima Y, Hosoda S: Idiopathic ventricular fibrillation induced with vagal activity in patients without obvious heart disease. Circulation 1997;95:2277-2285.

15. Matsuo K, Kurita T, Inagaki M, Kakishita M, Aihara N, Shimizu W, Taguchi A, Suyama K, Kamakura S, Shimomura K: The circadian pattern of the development of ventricular fibrillation in patients with Brugada syndrome. Eur Heart J 1999;20:465-470.

16. Scornik FS, Desai M, Brugada R, Guerchicoff A, Pollevick GD, Antzelevitch C, Pérez GJ: Functional expression of "cardiac-type" Nav1.5 sodium channel in canine intracardiac ganglia. Heart Rhythm 2006;3:842-850.

17. Makita N, Sumitomo N, Watanabe I, Tsutsui H: Novel SCN5A mutation (Q55X) associated with age-dependent expression of Brugada syndrome presenting as neurally mediated syncope. Heart Rhythm 2007;4:516-519.

18. Grimster A, Segal OR, Behr ER. Type 1 Brugada electrocardiogram pattern during the recovery phase of exercise testing. Europace 2008;10:897-898.

19. Miyazaki T, Mitamura H, Miyoshi S, Soejima K, Aizawa Y, Ogawa S: Autonomic and antiarrhythmic drug modulation of ST segment elevation in patients with Brugada syndrome. J Am Coll Cardiol 1996;27:1061-1070.

20. Nishizaki M, Sakurada H, Mizusawa Y, Niki S, Hayashi T, Tanaka Y, Maeda S, Fujii H, Ashikaga T, Yamawake N, Isobe M, Hiraoka M. Influence of meals on variations of ST segment elevation in patients with Brugada syndrome. J Cardiovasc Electrophysiol 2008;19:62-68.

21. Tan MP, Parry SW: Vasovagal syncope in the older patient. J Am Coll Cardiol 2008;51:599-606.

Structural Heterogeneity in the Ventricular Wall Plays a Significant Role in the Initiation of Stretch-Induced Arrhythmias in Perfused Rabbit Right Ventricular Tissues and Whole Heart Preparations

Kinya Seo, Masashi Inagaki, Satoshi Nishimura, Ichiro Hidaka, Masaru Sugimachi,
Toshiaki Hisada, Seiryo Sugiura

Rationale: Mechanical stress is known to alter the electrophysiological properties of the myocardium and may trigger fatal arrhythmias when an abnormal load is applied to the heart.

Objective: We tested the hypothesis that the structural heterogeneity of the ventricular wall modulates globally applied stretches to create heterogeneous strain distributions that lead to the initiation of arrhythmias.

Methods and Results: We applied global stretches to arterially perfused rabbit right ventricular tissue preparations. The distribution of strain (determined by marker tracking) and the transmembrane potential (measured by optical mapping) were simultaneously recorded while accounting for motion artifacts. The 3D structure of the preparations was also examined using a laser displacement meter. To examine whether such observations can be translated to the physiological condition, we performed similar measurements in whole heart preparations while applying volume pulses to the right ventricle. At the tissue level, larger stretches (≥20%) caused synchronous excitation of the entire preparation, whereas medium stretches (10% and 15%) induced focal excitation. We found a significant correlation between the local strain and the local thickness, and the probability for focal excitation was highest for medium stretches. In the whole heart preparations, we observed that such focal excitations developed into reentrant arrhythmias.

Conclusions: Global stretches of intermediate strength, rather than intense stretches, created heterogeneous strain (excitation) distributions in the ventricular wall, which can trigger fatal arrhythmias. (*Circ Res.* 2010;106:176-184.)

Key Words: stretch-induced arrhythmia ■ mechanoelectric feedback ■ optical mapping

Alterations to the mechanical state of the myocardium affect its electrophysiological properties, a phenomenon termed mechanoelectric feedback (MEF).[1,2] MEF is considered to play a significant role in the genesis of cardiac rhythm disturbances in various disease states, such as myocardial infarction and heart failure, in which myocardial tissues are subjected to abnormal loading conditions.[3–5] This speculation is supported by previous observations that in myocardial infarction, ventricular ectopic excitations are initiated by acute stretches of the border zone between the infarct and the normal myocardium.[6–8] A more definite causality is suspected in the etiology of commotio cordis, where sudden death occurs owing to a nonpenetrating chest wall impact in the absence of injury to the ribs, sternum, and heart.[9,10] Using anesthetized juvenile swine, Link et al[10] found that ventricular fibrillation can be produced by a baseball strike, and

examined the effects of the phase, strength and speed of the strike for the induction of arrhythmias.

To elucidate the mechanisms underlying MEF and related arrhythmias, extensive studies have been carried out using various preparations from various species, including rabbits, lambs and dogs.[11–13] Stretch-activated channels (SACs) have been regarded as the most likely candidates for the primary transducers of mechanical stress.[14–16] Although such findings at the molecular level can account for changes in the action potential duration, amplitude, effective refractory period and resting potential induced by mechanical interventions at the cellular level, we still face a huge gap between these laboratory findings and clinical arrhythmias observed at the organ level. In this context, Franz et al[17] investigated the effects of increases in ventricular volume and pressure on epicardial monophasic action potentials in both isolated cross-circulated hearts and
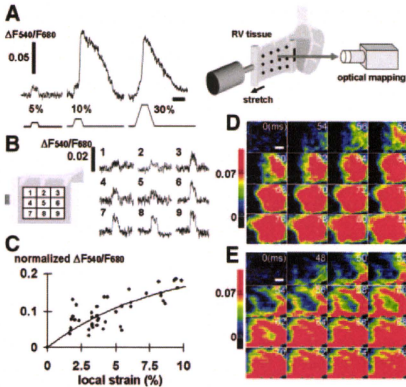
Figure 1. Alterations in the electric response in a cardiac tissue. A, Ratiometric optical signals ($\Delta F_{540}/F_{680}$) in response to 5%, 10%, and 30% stretches from left to right. Scale bar: 100 ms. B, Spatiotemporal pattern of the depolarizations (typical optical signals in each segment) in response to a 5% stretch. C, Relationship between the changes in the normalized optical signals and the local strain under the excitation threshold (n=5). The smooth curve through the data points was fitted with a nonlinear regression model. D and E, Representative action potentials and optical maps in response to 10% and 30% stretches, respectively. The stretch starts at 0 ms. Scale bar: 4 mm.

Non-standard Abbreviations and Acronyms	
MEF	mechanoelectric feedback
SAC	stretch-activated channel
RV	right ventricle

also examined. Similar measurements were conducted in whole heart preparations while applying acute volume pulses to the RV.

An expanded Methods section is available in the Online Data Supplement at http://circres.ahajournals.org.

Results

Effect of the Stretch Amplitude on Excitation of the Tissue

To elucidate the relationship between the electric response and the stretch level, we measured the optical transmembrane potential signals of stretched tissues. Figure 1 shows representative transmembrane potential signals in response to stretches of varying amplitudes. When a uniaxial stretch with a small amplitude (5%) was applied, the myocardial tissue was depolarized but an action potential did not develop (Figure 1A, left). The distribution of these depolarizations was heterogeneous and the amplitudes of these depolarizations had a positive dependence on the local strains (n=5) (Figure 1B and 1C). However, above a certain level of amplitude ($\geq$10%), we observed focal excitation (development of an action potential in less than 4 segments of 9 blocks) (Figure 1A, middle; Figure 1D). A larger stretch (30%) only induced multiple occurrences of excitation in the tissue (Figure 1E). Figure 2A shows the relationship between the probability of tissue excitation (development of an action potential in at least one locus within the tissue) and the amplitude of the stretch applied (global strain). We found a fairly abrupt transition in the tissue responses to a uniaxial stretch (n=7). Specifically, excitation was rare when the amplitude was small (5%), but its rate increased with stretches in the medium range (10% and 15%) to reach 100% (sure observation) in response to large stretches (20%, 25% and 30%).

The use of a trapezoidal command with constant rates of rise and fall necessarily made the entire duration of the stretch longer for larger stretches, which may thus have led to modulation of the responses of the myocardium through different mechanisms. To exclude these possibilities, we applied stretches of varying amplitudes while keeping the entire duration constant at 50 ms. We found similar responses, thereby indicating that the amplitude rather than the duration is the major determinant of stretch-induced activation of the myocardium (Online Figure V, A). We also confirmed that stretches applied during the action potentials could modulate their shapes, and sometimes found stretch-activated depolarizations followed by premature ventricular contractions (Online Figure V, B).

Relationship Between Stretch-Induced Excitation and Epicardial Local Strain

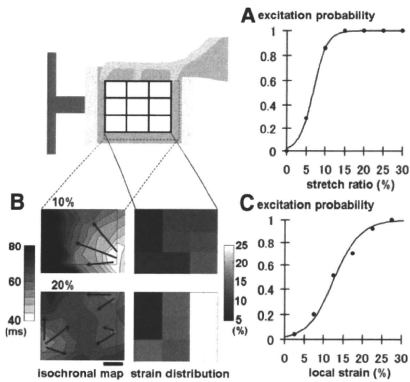We also evaluated the relevance between stretch-activated excitation and epicardial local strain (n=7). To compare the

in situ canine hearts to clearly demonstrate the manifestation of MEF. However, these volume and/or pressure alterations do not allow detailed evaluation of the changes in myocardial stress or strain, which are believed to be the keys for establishing a link between the macroscopic and microscopic phenomena.

To elucidate how the cellular responses to stretches lead to arrhythmias in the heart, we focused on the morphology of tissue preparations and its role in the modulation of the electric responses. We developed an experimental set-up in which controlled uniaxial stretches were applied to crystalline perfused rabbit ventricular walls while monitoring the local strain. The use of optical transmembrane potential mapping combined with a tissue tracking technique enabled us to examine the relationship between local strain and excitation of the myocardium. By applying acute stretches of varying amplitudes, we demonstrate that global stretches applied to the ventricular wall tissue can create strain dispersion in the heterogeneous structure of the ventricular wall and that mechanical insults of intermediate, rather than intense, strength induce focal excitation, thus potentially triggering fatal arrhythmias. Finally, using whole heart preparations, we confirm that only medium stretches of the myocardium can evoke spiral wave formation.

Methods

Japanese white rabbits weighing 2.4 to 2.9 kg were used. The distribution of strain and the transmembrane potential were simultaneously recorded while applying an acute stretch to right ventricle (RV) tissue preparations. The 3D structure of the preparations was

Figure 2. Electric responses and strain distributions. A, Probability that an action potential develops in at least 1 region of the whole tissue as a function of global stretch (n=7). The smooth curve through the data points was fit with a logistic regression model. B, Representative isochronal maps of a transmembrane potential showing the point of initial depolarization (left) and distributions of local strain (right). Top and bottom show 10% and 20% stretch, respectively. Scale bar: 4 mm. C, Relationship between the probability of stretch-induced excitation in the local area and the strain in the corresponding area (n=7). The smooth curve through the data points was fit with a logistic regression model.

Figure 3. Modulation of stretch-induced excitation by drugs. A, Effect of Gd^{3+} on the probability of stretch-induced excitation after a 15% stretch (n=7). *P<0.05. CTRL indicates control condition. B, Effect of ryanodine on the probability of stretch-induced excitation after a 15% stretch (n=3).

strain distribution with the isochronal electric responses, the whole tissue area was divided into 9 blocks and the average strain value in each block was shown in grayscale. The local strain maps at each level of stretch with the corresponding isochronal maps are shown in Figure 2B (right). Initial excitation tended to take place at the locus of high strain (top: right lower block with 14% strain; bottom: left lower block with 14% strain; right upper 2 blocks with 23% and 24% strains). The excitation probability was clearly found to be more prominent for higher strains (Figure 2C), when the probability of local excitation was plotted as a function of the corresponding local strain (n=7).

Involvement of SACs in Stretch-Induced Excitations

To examine the involvement of SACs in the genesis of stretch-induced excitation, we repeated the experiments with a 15% stretch in the presence of 10 μmol/L Gd^{3+}, a blocker of nonspecific SACs. Gd^{3+} inhibited the stretch-induced excitation by 71.4±18.4% compared with the control condition and its effect was reversed by washout of Gd^{3+} (Figure 3A; n=7; P<0.01, Gd(+) versus control condition and washout). We also administered ryanodine to examine whether stretch-induced Ca^{2+} release from the sarcoplasmic reticulum and the triggered activity are involved in the activation process. When we applied 15% stretches, action potentials developed similarly in both ryanodine-treated and untreated (control condition) tissues (Figure 3B; n=3).
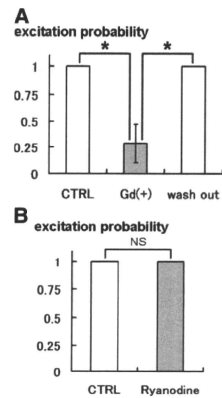
Strain Distribution and Tissue Structure

Because we applied uniaxial stretches to the ventricular tissue, the strain distribution on the epicardial surface was most probably created by heterogeneity within the tissue structure. To clarify the relationships between the strain distribution and the tissue structure, we measured the thickness distribution in each preparation using a laser displacement meter (Figure 4A; n=7). We divided the tissue into 9 blocks and calculated the average thickness in each block to facilitate comparisons with the strain data. Figure 4B shows a comparison between the thickness and local strain distributions after a 10% stretch from a single experiment. We found that the strain was high in regions where the tissue thickness was thin. For further comparisons between the tissue structure and the strain, we calculated the normalized thickness value of each block (mean thickness value of each block relative to the mean thickness value of all the blocks). Figure 4C summarizes the relationships between the local strain and the local thickness under different levels of stretch. Local strain was negatively correlated with the local thickness, which supported our hypothesis (10% stretch: n=7, r=−0.52, P<0.0001; 20% stretch: n=7, r=−0.53, P<0.0001).

Heterogeneous Excitation in Accordance With the Tissue Thickness and Stretch Level

We then plotted the relationship between the local wall thickness and the probability of stretch-induced local excitation for various levels of stretches (Figure 5A; n=7; closed circles, 5% stretch; closed triangles, 15% stretch; open circles, 30% stretch). When the applied stretch was small (5%), there was hardly any excitation (low probabilities over the entire range of thickness) because the local strain was below the threshold. As the amplitude of the stretch increased, the probability of excitation started to rise from the
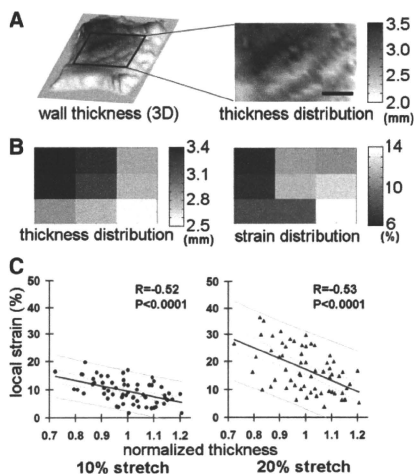
Figure 4. Thickness and local strain distributions of cardiac tissue. A, Representative case of the wall thickness distribution (laser-scanned data). Scale bar: 4 mm. B, Thickness distribution (left) and strain distribution (right) in response to a global 10% stretch in a representative experiment. C, Relationship between the normalized wall thickness and local strain in response to 10% (left) and 20% (right) global stretches. Lines are linear regression lines (10% stretch: n=7, r=−0.52, P<0.0001; 20% stretch: n=7, r=−0.53, P<0.0001).

Figure 5. Relationship between the probability of focal excitation and the stretch amplitude. A, Probabilities of stretch-induced local excitation as a function of the relative wall thickness for 5% (closed circles), 15% (closed triangles), and 30% (open circles) stretches (n=7). The smooth curves through the data points were fit with logistic regression models. Right, Distributions of the wall thicknesses, in which the segments where the action potentials developed are depicted in gray for 30% (top), 15% (middle), and 5% (bottom) stretches. B, From the data shown in A, the variability of the probability for the development of local excitation over the entire range of wall thickness was plotted as a function of the global stretch (n=7). Heterogeneous excitation is induced by a stretch of intermediate amplitude rather than a large stretch.

thin area (15%) and all areas were finally excited in response to a large stretch (30%). We calculated the variability (standard deviation) of the excitation probability over the entire thickness range for each stretch amplitude, and these data are plotted in Figure 5B (n=7). In regions of small (5%) or large (30%) stretches, the variability was low (0.18 or 0.26) because the whole tissue was either unresponsive or responsive to the stretch, respectively, whereas heterogeneous excitation was achieved in response to a stretch of intermediate amplitude (0.50 on 15% stretch).

Stretch-Induced Focal Excitations Develop Into Reentrant Arrhythmias in the Ventricle

To examine whether the findings at the tissue level are applicable to more physiological situations, we applied volume pulses to the RV in whole heart preparations and recorded the transmembrane potential responses. Figure 6A and 6B shows representative optical signals in response to 2 different amplitudes of volume pulses. When we applied a small volume pulse (0.5 mL), virtually no response was observed. However, local excitation (excitation from less than one-third of all the blocks) was induced by a 1.0-mL volume pulse (Figure 6A), and a large volume pulse (2.0 mL) elicited excitation from a larger area simultaneously (global excitation) (Figure 6B). The corresponding thickness distribution in the optically mapped region revealed that the focal excitation originated from a thin region (Figure 6C). As summarized in Figure 6D (n=6), focal excita-
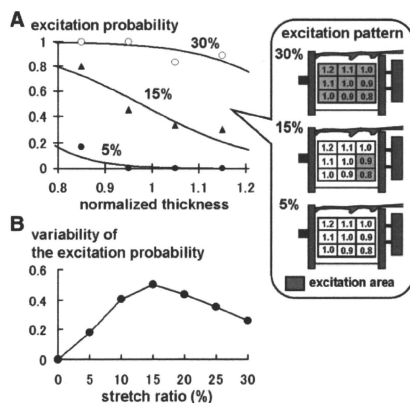
tion was only induced with pulses of intermediate volumes (1.0 and 1.5 mL). Structural measurements revealed that such focal excitations tended to take place in regions where the wall thickness was thinner (Figure 6E; n=6, P<0.05), similar to the case for the tissue preparations. All of these findings were in accordance with the tissue experiments, thus confirming that only global stretches of medium intensity can induce focal excitation in the ventricular wall.

Focal excitation is a prerequisite for the initiation of reentrant arrhythmias, but may not fulfill the conditions. Therefore, we hypothesized that when the propagation of the focal excitations induced by medium mechanical stimuli interacts with the preceding electric activations, it can develop into fatal reentrant arrhythmias. To assess this hypothesis, we applied the volume pulses to the RV for 50 ms at various coupling intervals (90 to 130 ms) with a preceding electric stimulus. Similar to the electric "pinwheel experiment" protocol,[18] this protocol involves the simultaneous establishment of a spatial gradient of momentary stretch-induced excitability together with a spatial gradient of refractoriness induced by the prior passage of an activation. As shown in Figure 7A, a 1.5-mL volume pulse after a 110-ms coupling interval initiated vortex-like reentrant waves pivoting around phase singularities. As clearly shown in Figure 7B, a large volume pulse (2.0 mL) never elicited arrhythmias, whereas an intermediate volume pulse (1.5 mL) applied after a proper coupling interval (110 ms) triggered reentrant arrhythmias (n=3, 66.7% probability).
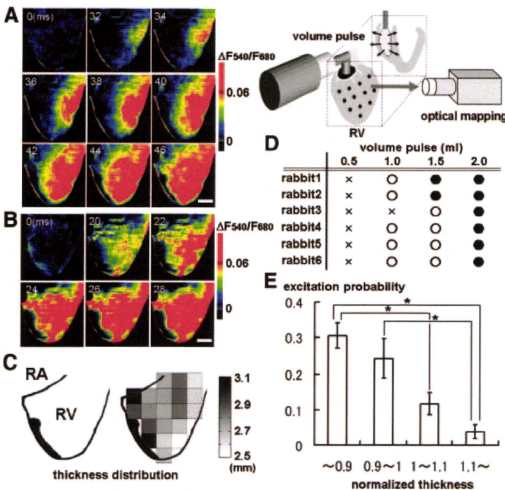
Figure 6. Alterations in the electric responses in a whole heart preparation. A and B, Representative optical maps of the responses of the RV to volume pulses of 1.0 mL (A) and 2.0 mL (B). The stretches start at 0 ms. Scale bar: 4 mm. C, Corresponding thickness distribution in the ventricle. RA indicates right atrium; RV, right ventricle. D, Response patterns to stretches in 6 rabbit hearts. Crosses indicate no excitation; focal excitation, open circles; global excitation, closed circles. E, Excitation probability for each normalized thickness range in the initiation of focal excitation (n=6). *P<0.05.

Discussion

In the present study, we simultaneously measured the transmembrane potentials and local strains while applying uniaxial stretches of varying amplitudes to rabbit RV wall tissue to clarify the linkage of electric activity between cells and organs. The use of optical transmembrane potential mapping coupled with local strain measurements based on bead markers enabled us to record the strain–electric response relationship of myocardial tissue. In addition, structural measurements of the preparations suggested that the complex architecture of the ventricular wall could cause heterogeneous strain responses to mechanical stimuli, thereby leading to the initiation of focal

excitation. We confirmed this hypothesis under more physiological conditions by successfully inducing reentrant arrhythmias using a volume pulse of medium amplitude.

Optical Mapping of the Transmembrane Potential

Owing to its high temporal and spatial resolutions, optical recording of transmembrane potentials has been widely used, but most studies have only dealt with immobile preparations where the motion was inhibited mechanically and/or pharmacologically.[19–21] These stabilizations of the preparations were conducted to prevent motion artifacts caused by changes in the fluorescence intensity along the light path, and also
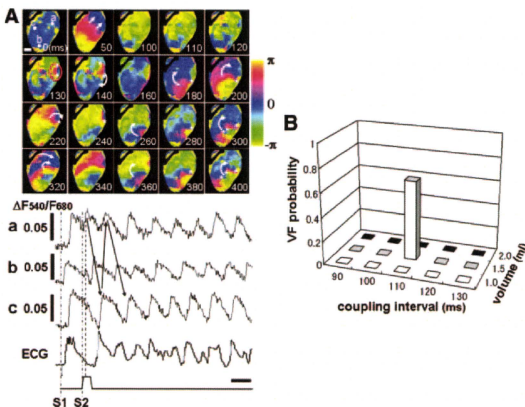

Figure 7. Initiation of spiral waves by volume pulses. A, Representative phase maps of spiral wave formation. The volume pulse was applied at 110 ms after the electric stimulus. Scale bar: 4 mm. a through c represent the ratiometric optical signals (ΔF540/F680) for the corresponding positions shown in the 0-ms optical map (top left). The electric stimulus starts at 0 ms. The ECG is shown at the bottom. Scale bar: 100 ms. *Phase singularity points. B, Excitation probabilities in relation to the coupling intervals and the intensities of the volume pulses (n=3).

changes in the x-y position. In the present study, we tried to account for the motion-induced contamination of optical signals by using 2 methods to accurately evaluate the transmembrane potentials of the local myocardium while applying a stretch to the whole tissue. First, the fluctuation of light intensity was cancelled by ratiometry of the 2 emission bands of the fluorescent indicators. Second, by using the affine transformation based on motion tracking, we successfully traced the tissue points, presumably a cluster of specific myocytes, during a stretch and induced contraction, and showed the sequential changes in the transmembrane potential in the reference plane. As shown in Figure 1A, the local action potential triggered by the stretch reconstructed with these techniques is similar to that recorded by an electrode with its clear zero phase characteristics. Compared with a previous study of the local response of electric activity to a linear acute stretch using a pair of electrodes in isolated frog ventricular tissue at only 2 points,[22] detailed maps of the action potentials were obtained with the present technique.

Heterogeneity in the Tissue Structure for Bridging Cellular Responses to Arrhythmias

Although the activity of ion channels was not directly measured, the present results were consistent with previous studies demonstrating the involvement of SACs in MEF. Zeng et al[23] recorded the stretch-dependent inward current, which was blocked by Gd^{3+} in rat cardiac myocytes. They also observed that a 10% stretch induced an immediate contraction of the myocytes. Although the threshold for excitation varies among studies, similar observations were made for rat ($>20\%$),[24] guinea pig (20% to 25%),[25] and frog (15%)[26] myocytes. In our probability curves of stretch-induced excitation for both whole tissues and segments (Figure 2A and 2C), the transition from nonresponse to excitation took place within a similar range of stretch amplitudes. Furthermore, the response was inhibited by Gd^{3+} and recovered by washout of the agent. Taken together, these results suggest that a uniaxial stretch applied to the tissue induces strain in the myocytes, which in turn triggers the activation of molecular mechanotransducers, most probably SACs.

The use of a tissue preparation provided us with a unique opportunity to elucidate the relationships among electric excitation, global strain and local strain on the epicardial surface. Although a uniaxial global stretch was applied to the preparation, excitation was usually only induced in a limited area where the local strain was high. We speculate that such heterogeneity in the strain distribution reflects the complex structure of the ventricular wall, such that the excitation is initiated in regions where the wall is thin. Whereas the complex structure of the ventricles normally allows vigorous contraction, different hemodynamic overloads in diseased states lead to abnormalities in the ventricular shape and regional wall motion,[27,28] which may sometimes evoke focal excitations.

We must consider the possibility that the presence of damaged ends may have caused an abnormal strain near the tissue supports to initiate the excitation from the edge region. However, the locus of focal excitation always followed the thickness distribution, such that the excitation was elicited in the center of a preparation that had a thin central region (Online Figure VI, A). Furthermore, ter Keurs et al[29] reported that stretch-induced excitations from the damaged myocardium occur through a calcium-related triggering mechanism, and that Gd^{3+} does not suppress these phenomena.

We also considered the relevance of a Ca^{2+}-related mechanism to our experiments. Fujiwara et al[30] showed that triggered activities were subsequently evoked by a Ca^{2+} release from the sarcoplasmic reticulum through ryanodine receptors. Furthermore, some previous studies reported that an acute stretch can also trigger a Ca^{2+} release from the sarcoplasmic reticulum through ryanodine receptors.[31,32] In our experiments, however, the stretch-induced excitations were still observed after administration of ryanodine. Moreover, changes in the extracellular calcium concentration did not affect the stretch-induced excitability. These observations indicate that the stretch-induced excitations in our experiments were not linked to calcium-related membrane activations like the triggered activities. Wakayama et al[33] also reported that excitation caused by MEFs can be the consequence of a quick stretch release, which is related to stretch-dependent binding and release of Ca^{2+} to contractile proteins. In our experiments, however, the excitations were initiated during the rise or plateau of the stretches, and not during the release of the stretches (Figure 1A, right). This discrepancy may be caused by the fact that the excitation as a consequence of a quick release in the previous report was only observed at a high Ca^{2+} concentration (5.2 ± 0.73 mmol/L), whereas our experiments were carried out with a lower Ca^{2+} concentration (1.8 mmol/L). These observations indicate that the stretch-induced excitations observed in our study are not related to the release of Ca^{2+} to contractile proteins following the stretch release.

Translation of data obtained with tissue preparations to the intact heart requires consideration in terms of both the magnitude and the nature of the deformation. A volume pulse of 2.0 mL induced global excitation, the effect caused by a 20% stretch of the tissue. However, if we simply assume a spherical ventricle, a 20% increase in its circumference would lead to an almost 70% increase in its volume, which cannot be accounted for by the 2.0-mL volume pulse in the rabbit RV. We can speculate that the thinner RV free wall was preferentially stretched whereas the thick ventricular septum remained unchanged. In addition to the stretch applied to the tissue preparations, volume expansion of the ventricle also causes shear and compression of the wall. In fact, Isenberg et al[34] revealed that stretch and compression activated different ion currents in guinea pig ventricular myocytes. Furthermore, Gopalan et al[35] reported that transverse stretches have more pronounced effects on mechanotransduction signaling pathways. This may be associated with the stretch sensitivity regarding the spatial distributions of SACs and cytoskeletal structures. Although currents and cytoskeletal structures were not examined in the present study, such aspects should be addressed in future studies.

Modulation of Transmembrane Potentials and Conduction Velocity by the Stretches

Although we focused on the magnitude of the stretch in the present study, care was taken to eliminate confounding

factors. Fasciano and Tung[22] revealed that the stretch speed significantly affects the stretch-induced excitability. In this context, we made the speed of the stretch constant in all the experiments (Online Figure IV). We checked the influence of the stretch duration in another set of experiments in which the stretch duration was made constant at 50 ms. We confirmed that these 2 types of protocols did not cause any significant differences in the excitability induced by the stretch.

We also examined the effect of the stretch timing relative to the action potentials. Similar to previous reports,[17,36] stretches applied in each phase (2, 3 and 4) of the action potentials modulated the transmembrane potentials differently (Online Figure V, B).

We calculated the conduction velocity of the focal excitations elicited by 10% stretches and compared it with that elicited by an electric stimulus (Online Figure VI, B). In these experiments, the spread of conduction between 2 recording positions (crosses) was completed during the stretch plateau. Although the number of observations was limited owing to the technical difficulty, we confirmed that the conduction velocities of the stretch-induced excitations in both the horizontal and vertical directions tended to be slower (31.7% and 38.7% decrease in vertical and horizontal direction, respectively). In addition, we also examined the relationship between the normalized dV/dt_{max} (evaluated by the time derivative of the ratiometric optical signal, dF/dt_{max}) of action potential upstrokes and local strains. Normalized dV/dt_{max} of the action potential upstroke was decreased in regions where local strain was high (Online Figure VII). Although the effects of stretches on the conduction velocity are still controversial,[37] conduction slowing has been reported in previous studies.[21,38] Eijsbouts et al[38] reported that the anisotropic nature in the heterogeneous wall thickening may play an important role in conduction disturbances attributable to dilation. Geometric and structural changes during an acute stretch should be some of the causes of this effect, and SACs and the intracellular calcium dynamics may also be involved in this phenomenon. In either case, such changes in the propagation characteristics could also contribute to the development of reentrant arrhythmias.

Clinical Implications

When a mechanical stimulus of moderate amplitude was applied to the ventricular wall, local excitation was induced in regions where the wall thickness was thin and, if other facilitatory conditions were met, it was propagated to the adjacent area to develop into fatal arrhythmias. We expect that further increases in the intensity of the stimulus would induce multiple excitations to exaggerate the electric heterogeneity, thereby increasing the possibility of arrhythmias. However, if a very intense stimulus is applied, the whole tissue can be synchronously excited, which considerably decreases the possibility of arrhythmias (Figure 5B). Interestingly, we can see a similar tendency in the relationship between the ventricular fibrillation probability and the rise in ventricular pressure produced by a baseball impact in an experimental study on commotio cordis by Link et al,[10] who did not provide any mechanistic comments.

In this study, a volume pulse of 1.5 mL at a 110-ms coupling interval after the last electric stimulus initiated a reentrant arrhythmia. No reentrant arrhythmia, however, was induced by 1.0-mL volume pulses that triggered focal excitations when applied at 500-ms coupling intervals. These findings probably arise from a dependence of the strength of the mechanical stimuli required to generate focal activity on the phase of the action potential at which it is applied. In contrast to the protocol (a), in which the pulses were applied to the fully relaxed ventricle after a long coupling interval (500 ms), we confirmed that the myocardium in activated states has higher thresholds for activation (Online Figure VIII). Based on these observations, a 1.0-mL volume pulse cannot initiate the excitation with coupling intervals from 90 to 130 ms, whereas a 1.5-mL volume pulse can initiate focal excitations with coupling intervals of >100 ms. Although the focal excitations were frequently initiated with coupling intervals of >120 ms, the excitations did not develop into reentrant arrhythmias because a unidirectional conduction block cannot be formed at these timings. Owing to the trapezoidal volume change and viscoelastic nature of the tissue, the effect of the volume pulse was realized with some delay. In fact, although we applied a volume pulse after a 110-ms coupling interval, excitation was initiated at around 130 ms corresponding to the late phase 2 of the action potential. We speculate that these findings correspond to the observation that ventricular fibrillations were triggered when the chest wall impacts were applied during the vulnerable portion of the T wave.[9]

Our present results suggest that the complex structure of the ventricular wall functions to modulate a mechanical impact and create a heterogeneous excitation distribution in response to a stimulus of intermediate intensity, rather than an intense stimulus, to initiate ventricular fibrillation in otherwise healthy young subjects.

The structural complexity of the ventricular wall may also contribute to the genesis of arrhythmias in old myocardial infarctions. Regarding myocardial infarction, it is considered that the conduction abnormality in the infarct area acts as the substrate for arrhythmias,[39] but its trigger still remains unclear. Bogen et al[40] reported that a large mechanical load is added to the border zone in regions where the wall thickness is thin in systole. Moreover, Josephson[41] revealed that arrhythmias are often initiated from these borders. Calkins et al[8] observed that ventricular dilation shortens the refractoriness of the surviving myocardium in the infarct area rather than the healthy myocardium. Taken together, the following scenario is conceivable. In an old myocardial infarction, a systolic rise in ventricular pressure can induce a large stretch in the functional border zone, where the wall thickness is thin to provoke an ectopic excitation, which may develop into fatal reentrant arrhythmias promoted by the conduction abnormality in the infarct area.

In either case, the structural and/or functional heterogeneity of the myocardial tissue serves to create a heterogeneous strain distribution, and establishes a MEF-mediated electrophysiological dispersion in the tissue, which is known to be a potent substrate for arrhythmias.

Study Limitations

Although the use of flattened tissue preparations made it easy to evaluate local strain, the results cannot be translated directly to the clinical setting where volume/pressure loading or external compression distorts the ventricular tissue in a complex manner. Furthermore, although uniaxial stretches may cause 3D strain within the tissue with reductions in the width and thickness, these effects were not taken into consideration. On the other hand, the intact heart preparations pose a problem for potential mapping and the measurement of strain. In either case, because the action potentials and strains were recorded at the epicardial surface, we did not evaluate the heterogeneity in the transmural structure from the epicardium to the endocardium. Furthermore, as stated above, we did not measure the ion currents in response to the stretches, although they seemed to greatly promote our understanding of stretch-induced arrhythmias in the intact heart. Finally, we only used the RV in our experiments based on our assumption that the RV is more vulnerable to mechanical stimuli because of its weak elasticity, and stretch-induced arrhythmias could also be evoked in the left ventricle.

In summary, a global stretch applied to the ventricular wall tissue can create a heterogeneous strain distribution in the heterogeneous structure of the ventricular wall. Such heterogeneity in the strain distribution can lead to local excitation, which in turn leads to fatal reentrant arrhythmias.

Sources of Funding

Disclosures

None.

References

1. Taggart P, Lab M. Cardiac mechano-electric feedback and electrical restitution in humans. *Prog Biophys Mol Biol.* 2008;97:452–460.
2. Ravens U. Mechano-electric feedback and arrhythmias. *Prog Biophys Mol Biol.* 2003;82:255–266.
3. Tomaselli GF, Marban E. Electrophysiological remodeling in hypertrophy and heart failure. *Cardiovasc Res.* 1999;42:270–283.
4. Janse MJ. Electrophysiological changes in heart failure and their relationship to arrhythmogenesis. *Cardiovasc Res.* 2004;61:208–217.
5. Aimond F, Alvarez JL, Rauzier JM, Lorente P, Vassort G. Ionic basis of ventricular arrhythmias in remodeled rat heart during long-term myocardial infarction. *Cardiovasc Res.* 1999;42:402–415.
6. Coronel R, Wilms-Schopman FJ, deGroot JR. Origin of ischemia-induced phase 1b ventricular arrhythmias in pig hearts. *J Am Coll Cardiol.* 2002;39:166–176.
7. Dillon SM, Allessie MA, Ursell PC, Wit AL. Influences of anisotropic tissue structure on reentrant circuits in the epicardial border zone of subacute canine infarcts. *Circ Res.* 1988;63:182–206.
8. Calkins H, Maughan WL, Weisman HF, Sugiura S, Sagawa K, Levine JH. Effect of acute volume load on refractoriness and arrhythmia development in isolated, chronically infarcted canine hearts. *Circulation.* 1989; 79:687–697.
9. Link MS, Wang PJ, Pandian NG, Bharati S, Udelson JE, Lee MY, Vecchiotti MA, VanderBrink BA, Mirra G, Maron BJ, Estes NA III. An

experimental model of sudden death due to low-energy chest-wall impact (commotio cordis). *N Engl J Med.* 1998;338:1805–1811.
10. Link MS, Maron BJ, Wang PJ, VanderBrink BA, Zhu W, Estes NA III. Upper and lower limits of vulnerability to sudden arrhythmic death with chest-wall impact (commotio cordis). *J Am Coll Cardiol.* 2003;41: 99–104.
11. Chen RL, Penny DJ, Greve G, Lab MJ. Stretch-induced regional mechanoelectric dispersion and arrhythmia in the right ventricle of anesthetized lambs. *Am J Physiol Heart Circ Physiol.* 2004;286:H1008–H1014.
12. Hansen DE, Craig CS, Hondeghem LM. Stretch-induced arrhythmias in the isolated canine ventricle. Evidence for the importance of mechanoelectrical feedback. *Circulation.* 1990;81:1094–1105.
13. Parker KK, Taylor LK, Atkinson JB, Hansen DE, Wikswo JP. The effects of tubulin-binding agents on stretch-induced ventricular arrhythmias. *Eur J Pharmacol.* 2001;417:131–140.
14. Sachs F. Stretch-activated channels in the heart. In: Kohl P, Sachs F, Franz MR, eds. *Cardiac Mechano-Electric Feedback and Arrhythmias: From Pipette to Patient.* Philadelphia, Pa: Elsevier Sauders; 2005;2–10.
15. Ward ML, Williams IA, Chu Y, Cooper PJ, Ju YK, Allen DG. Stretch-activated channels in the heart: contributions to length-dependence and to cardiomyopathy. *Prog Biophys Mol Biol.* 2008;97:232–249.
16. Kohl P, Day K, Noble D. Cellular mechanisms of cardiac mechanoelectric feedback in a mathematical model. *Can J Cardiol.* 1998;14: 111–119.
17. Franz MR, Burkhoff D, Yue DT, Sagawa K. Mechanically induced action potential changes and arrhythmia in isolated and in situ canine hearts. *Cardiovasc Res.* 1989;23:213–223.
18. Winfree AT. Electrical instability in cardiac muscle: phase singularities and rotors. *J Theor Biol.* 1989;138:353–405.
19. Kanai A, Salama G. Optical mapping reveals that repolarization spreads anisotropically and is guided by fiber orientation in guinea pig hearts. *Circ Res.* 1995;77:784–802.
20. Moreno J, Zaitsev AV, Warren M, Berenfeld O, Kalifa J, Lucca E, Mironov S, Guha P, Jalife J. Effect of remodelling, stretch and ischaemia on ventricular fibrillation frequency and dynamics in a heart failure model. *Cardiovasc Res.* 2005;65:158–166.
21. Sung D, Mills RW, Schettler J, Narayan SM, Omens JH, McCulloch AD. Ventricular filling slows epicardial conduction and increases action potential duration in an optical mapping study of the isolated rabbit heart. *J Cardiovasc Electrophysiol.* 2003;14:739–749.
22. Fasciano RW II, Tung L. Factors governing mechanical stimulation in frog hearts. *Am J Physiol.* 1999;277:H2311–H2320.
23. Zeng T, Bett GC, Sachs F. Stretch-activated whole cell currents in adult rat cardiac myocytes. *Am J Physiol Heart Circ Physiol.* 2000;278: H548–H557.
24. Nishimura S, Kawai Y, Nakajima T, Hosoya Y, Fujita H, Katoh M, Yamashita H, Nagai R, Sugiura S. Membrane potential of rat ventricular myocytes responds to axial stretch in phase, amplitude and speed-dependent manners. *Cardiovasc Res.* 2006;72:403–411.
25. Kamkin A, Kiseleva I, Isenberg G. Stretch-activated currents in ventricular myocytes: amplitude and arrhythmogenic effects increase with hypertrophy. *Cardiovasc Res.* 2000;48:409–420.
26. Tung L, Sliz N, Mulligan MR. Influence of electrical axis of stimulation on excitation of cardiac muscle cells. *Circ Res.* 1991;69:722–730.
27. Katz AM, Katz PB. Homogeneity out of heterogeneity. *Circulation.* 1989;79:712–717.
28. Remme EW, Nasb MP, Hunter PJ. Distributions of myocytes stretch, stress, and work in models Of normal and infarcted ventricles. In: Kohl P, Sachs F, Franz MR, eds. *Cardiac Mechano-Electric Feedback and Arrhythmias: From Pipette to Patient.* Philadelphia, Pa: Elsevier Sauders; 2005;381–391.
29. ter Keurs HE, Zhang YM, Miura M. Damage-induced arrhythmias: reversal of excitation-contraction coupling. *Cardiovasc Res.* 1998;40: 444–455.
30. Fujiwara K, Tanaka H, Mani H, Nakagami T, Takamatsu T. Burst emergence of intracellular Ca2+ waves evokes arrhythmogenic oscillatory depolarization via the Na+-Ca2+ exchanger: simultaneous confocal recording of membrane potential and intracellular Ca2+ in the heart. *Circ Res.* 2008;103:509–518.
31. Iribe G, Ward CW, Camelliti P, Bollensdorff C, Mason F, Burton RA, Garny A, Morphew MK, Hoenger A, Lederer WJ, Kohl P. Axial stretch of rat single ventricular cardiomyocytes causes an acute and transient increase in Ca2+ spark rate. *Circ Res.* 2009;104:787–795.

32. Tatsukawa Y, Kiyosue T, Arita M. Mechanical stretch increases intracellular calcium concentration in cultured ventricular cells from neonatal rats. *Heart Vessels.* 1997;12:128–135.

33. Wakayama Y, Miura M, Sugai Y, Kagaya Y, Watanabe J, ter Keurs HE, Shirato K. Stretch and quick release of rat cardiac trabeculae accelerates Ca2+ waves and triggered propagated contractions. *Am J Physiol Heart Circ Physiol.* 2001;281:H2133–H2142.

34. Isenberg G, Kazanski V, Kondratev D, Gallitelli MF, Kiseleva I, Kamkin A. Differential effects of stretch and compression on membrane currents and [Na+]c in ventricular myocytes. *Prog Biophys Mol Biol.* 2003;82: 43–56.

35. Gopalan SM, Flaim C, Bhatia SN, Hoshijima M, Knoell R, Chien KR, Omens JH, McCulloch AD. Anisotropic stretch-induced hypertrophy in neonatal ventricular myocytes micropatterned on deformable elastomers. *Biotechnol Bioeng.* 2003;81:578–587.

36. Zabel M, Koller BS, Sachs F, Franz MR. Stretch-induced voltage changes in the isolated beating heart: importance of the timing of stretch and implications for stretch-activated ion channels. *Cardiovasc Res.* 1996;32: 120–130.

37. Mills RW, Narayan SM, McCulloch AD. The effects of wall stretch on ventricular conduction and refractoriness in the whole heart. In: Kohl P, Sachs F, Franz MR, eds. *Cardiac Mechano-Electric Feedback and Arrhythmias: From Pipette to Patient.* Philadelphia, Pa: Elsevier Sauders; 2005;127–136.

38. Eijsbouts SC, Majidi M, van Zandvoort M, Allessie MA. Effects of acute atrial dilation on heterogeneity in conduction in the isolated rabbit heart. *J Cardiovasc Electrophysiol.* 2003;14:269–278.

39. Aizawa M, Aizawa Y, Chinushi M, Takahashi K, Shibata A. Conductive property of the zone of slow conduction of reentrant ventricular tachycardia and its relation to pacing induced terminability. *Pacing Clin Electrophysiol.* 1994;17:46–55.

40. Bogen DK, Rabinowitz SA, Needleman A, McMahon TA, Abelmann WH. An analysis of the mechanical disadvantage of myocardial infarction in the canine left ventricle. *Circ Res.* 1980;47:728–741.

41. Josephson ME, Harken AH, Horowitz LN. Endocardial excision: a new surgical technique for the treatment of recurrent ventricular tachycardia. *Circulation.* 1979;60:1430–1439.